Journal of Controlled Release 309 (2019) 181–189

Contents lists available at ScienceDirect

Journal of Controlled Release

journal homepage: www.elsevier.com/locate/jconrel

Co-delivery of therapeutic protein and catalase-mimic nanoparticle using a biocompatible nanocarrier for enhanced therapeutic effect

Seoungkyun Kim[1], Manse Kim[1], Secheon Jung, Kiyoon Kwon, Junyong Park, Sukhwan Kim, Inchan Kwon*, Giyoong Tae*

School of Materials Science and Engineering, Gwangju Institute of Science and Technology (GIST), Gwangju 61005, Republic of Korea

ARTICLE INFO

Keywords:
Therapeutic proteins
Uricase
Gold nano-particles
Pluronic-based nano-carrier
Co-delivery

ABSTRACT

Therapeutic proteins are indispensable in the treatment of various human diseases. Despite the many benefits of therapeutic proteins, they also exhibit diverse side effects. Therefore, reducing unwanted side effects of therapeutic proteins as well as enhancing their therapeutic efficacy are very important in developing therapeutic proteins. Urate oxidase (UOX) is a therapeutic enzyme that catalyzes the conversion of uric acid (UA) into a soluble metabolite, and it is used clinically for the treatment of hyperuricemia. Since UA degradation by UOX generates H_2O_2 (a cytotoxic side product), UOX was co-delivered with catalase-mimic nanoparticles (AuNPs) using biocompatible pluronic-based nanocarriers (NCs) to effectively reduce H_2O_2-associated toxicity in cultured cells and to enhance UA degradation efficiency *in vivo*. Simple temperature-dependent size changes of NCs allowed co-encapsulation of both UOX and AuNPs at a high loading efficiency without compromising critical properties, resulting in efficient modulation of a mixing ratio of UOX and AuNPs encapsulated in NCs. Co-localizing UOX and AuNPs in the NCs led to enhanced UA degradation and H_2O_2 removal *in vitro*, leading to a great reduction in H_2O_2-associated cytotoxicity compared with UOX alone or a free mixture of UOX and AuNPs. Furthermore, we demonstrated that co-delivery of UOX and AuNPs using NCs significantly improves *in vivo* UA degradation compared to simple co-injection of free UOX and AuNPs. More broadly, we showed that biocompatible pluronic-based nanocarriers can be used to deliver a target therapeutic protein along with its toxicity-eliminating agent in order to reduce side effects and enhance efficacy.

1. Introduction

Therapeutic proteins are used for clinical treatment of diverse human diseases [1–6] because of their favorable features including great biocompatibility, selectivity, and efficacy compared with chemical drugs [7]. However, therapeutic proteins can also cause side effects, such as headache, diarrhea, transient rash, cytopenias, cardiac toxicity, hypertension, anaphylaxis, exfoliative dermatitis, immunogenicity, and serum sickness [8–10]. Reducing side effects is a critical issue in developing therapeutic proteins, along with other, conventional issues, such as enhancing therapeutic efficacy and stability. To date, in order to reduce doses of therapeutic proteins and consequently lessen their side effects, alteration of amino acid composition or conjugation of a biocompatible molecule (*e.g.*, polyethylene glycol [PEG]) has been widely applied [11–17]. Since these approaches may compromise critical properties of therapeutic proteins, developing alternative strategies is required.

Herein, we investigated whether the co-delivery of therapeutic protein and catalytic nanoparticles using nanocarriers has a potential to mitigate toxicity-related side-effects, while maintaining the efficacy of the therapeutic protein both *in vitro* and *in vivo* (Fig. 1). We chose urate oxidase (UOX) as a model therapeutic protein; it is a therapeutic enzyme catalyzing the conversion of insoluble uric acid (UA) into soluble 5-hydroxyisourate (5-HIU). UOX is used to treat hyperuricemia associated with gout, kidney diseases, cardiovascular diseases, and tumor lysis syndrome (TLS) [18–20]. TLS can occur during the treatment of cancer when many tumor cells are lysed. Gout is a common inflammatory arthritis caused by the deposition of uric acid (UA) crystals in joints and soft tissues. Prevalence of gout varies from 0.1 to 10% of population among countries [21]. The conversion of UA to 5-HIU catalyzed by UOX also generates H_2O_2, which is toxic and can cause an adverse effect for patients who are glucose-6-phophate dehydrogenase deficient (Fig. 1(a)) [22]. Gold nanoparticles (AuNP) are highly biocompatible metals, and they are known to degrade H_2O_2 like catalase

* Corresponding authors at: Gwangju Institute of Science and Technology, School of Materials Science and Engineering, Gwangju 61005, Republic of Korea.
E-mail addresses: inchan@gist.ac.kr (I. Kwon), gytae@gist.ac.kr (G. Tae).
[1] These authors equally contributed to this manuscript.

https://doi.org/10.1016/j.jconrel.2019.07.038
Received 17 April 2019; Received in revised form 24 July 2019; Accepted 25 July 2019
Available online 26 July 2019

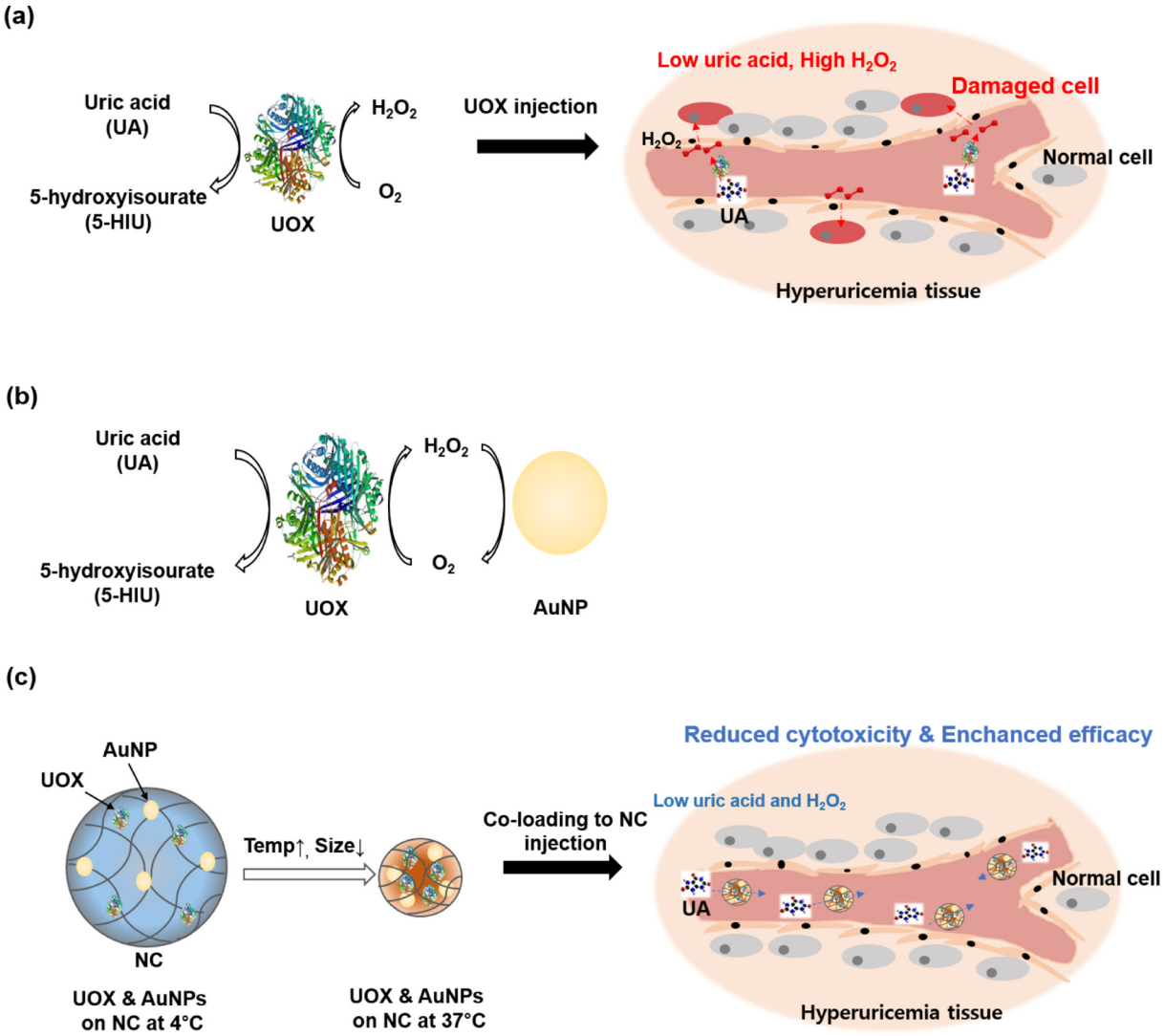

Fig. 1. Schemes of administration of UOX and AuNPs for hyperuricemia treatment. (a) Administration of the free UOX. (b) Cascade reaction between UOX and AuNP. (c) Administration of the UOX and AuNPs encapsulated in NCs.

[23]. In our previous study, we demonstrated that catalase-mimic AuNPs can reduce the H_2O_2 level generated from the conversion of UA by UOX [24]. Reduction in H_2O_2 level was expected to shift the equilibrium state toward a lower UA level. Therefore, the use of AuNPs led to an increase in degradation of UA by removing H_2O_2 and supplying extra O_2 to the UOX (Fig. 1(b)). Such enzyme-mimic nanoparticles are called nanozyme [25]. Nanozymes have received attention as an alternative of enzymes because of their high stability and cost-effectiveness compared with enzymes [26]. However, enzyme-nanozyme systems have been mainly used in biosensor area [27] or nanozyme alone [28–30] because they have limitations for *in vivo* application. For example, although the use of catalase-mimic AuNPs with UOX reduced H_2O_2 level *in vitro*, their applications *in vivo* are challenging. Upon the administration of UOX and AuNPs in blood, their concentrations are diluted to a very low concentration. Therefore, they cannot be located close enough to each other to achieve efficient cascade reactions composed of 1) generation of H_2O_2 by UOX and 2) removal of H_2O_2 by AuNPs. In order side-product H_2O_2 to be removed efficiently by AuNPs, AuNPs and UOX need to be delivered together in a single carrier.

As delivery carrier, metal-organic frameworks (MOFs) and mesoporous silica nanoparticles (MSN) have been used for proteins and nanomaterials together [31,32]. Briefly, Zhou and co-workers had designed the enzyme and gold nanoparticles to be loaded by MOFs, and then a chain reaction takes place. Through this, they had developed a sensor that measures changes in the concentration of substances in the body [31]. In another design, Qu and co-workers utilized MSNs for carrying of the enzyme and PtNPs [32]. However, these carriers may have issues, such as potential toxicity of MOFs and MSNs [33–36]. Also activity loss of the loaded enzymes due to harsh preparation/loading conditions may have disadvantages. Furthermore, it was challenging to modulate the amount of proteins/nanomaterials loaded to MOFs and MSNs, due to varying loading efficiencies dependent of type of materials.

In this study, we employed thermosensitive, biocompatible pluronic-based NCs. Previously, we developed pluronic-based NCs using photocrosslinking of pluronic and applied them as an efficient *in vivo* drug delivery system [37–40]. Based on their large size change upon temperature change (volume expansion ~ 10^3 times from 37 °C to 4 °C) and surfactant properties of pluronic [37], various biomacromolecules and metal nanomaterials-such as bovine serum albumin, basic fibroblast growth factor, vascular endothelial growth factor, bone morphogenetic protein, lysozyme, iron oxide nanoparticles, gold nanorods, and gold nanoparticle-could be loaded very efficiently and easily by simple coincubation in aqueous solutions at a low temperature, followed by a temperature increase to 37 °C [37,40–42]. In addition, biomolecules encapsulated in the NCs preserved their bioactivity

during long-term incubation under physiological conditions, and the loaded NCs showed good stability in serum containing environments [38,40–42]. Furthermore, since the NCs can encapsulate several substances simultaneously [43], they can be capable of delivering two or more complementary substances. In addition, since the loading efficiency of proteins and nanomaterials into pluronic based NCs was very high (over 90%) [37,42], the amount of loaded proteins and nanomaterials could be easily modulated. Thus, we hypothesized that co-delivery of UOX and AuNPs in the pluronic based NCs would be able to achieve efficient degradation of UA *in vivo*, due probably to efficient H_2O_2 removal *in situ* (Fig. 1(c)). The effects of co-localization of UOX and AuNPs using the NCs were systematically characterized *in vitro* as well as *in vivo* using a hyperuricemia mice model.

2. Materials and methods

2.1. Materials

Gold nanoparticles (diameter: 5 nm) coated with poly(vinylpyrrolidone) were purchased from nanoComposix Inc. (San Diego, CA). Ni-nitrilotriacetic acid (Ni-NTA) resins ware purchased from Qiagen (Valencia, CA, USA). Vivaspin centrifugal concentrators with a molecular weight cut-off (MWCO) of 50 kDa were purchased from Sartorius Corporation (Bohemia, NY, USA). PD-10 desalting columns were purchased from GE Health care (Piscataway, NJ, USA). Yeast extract, tryptone, and agar were obtained from DB Biosciences (San Jose, CA, USA). Pluronic F127, a poly(ethylene oxide)-poly(propylene oxide)-poly(ethylene oxide) (PEO-PPO-PEO) (PEO100-PPO65-PEO100, molecular weight: 12.6 kDa) was kindly donated by BASF Corporation (Seoul, South Korea). Acryloyl chloride was bought from Tokyo Chemical Industry (TCI, Tokyo, Japan). 4-(2-Hydroxyethoxy) phenyl-(2-hydroxy-2Propyl) ketone (Irgacure 2959) was obtained from Ciba Specialty Chemicals Inc. (Basel, Switzerland). Nanosep® centrifugal devices for spin-filtration (MWCO 300 kDa) were purchased from Pall Life Sciences (Ann Arbor, MI, USA). All other reagents were purchased from Sigma-Aldrich (Saint Louis, MO, USA), unless otherwise noted. All reagents were analytical grade and used without further purification.

2.2. Expression and purification of UOX

The plasmid encoding a gene of recombinant urate oxidase derived from *Aspergillus flavus* under control of T5 promoter (pQE80-UOX) was transformed into TOP10 *Escherichia coli* cells as reported previously [44]. Pre-cultured transformant cells were inoculated into a fresh 2xYT medium with 100 μg/mL ampicillin, and then cultured with shaking (220 rpm) at 37 °C. When the optical density at 600 nm (OD_{600nm}) reached 0.5, 1 mM of isopropyl β-D-1-thiogalactopyranoside was added to the culture for induction of UOX expression followed by incubation for 5 h. Then, the cells were pelleted by centrifugation at 6000 rpm for 10 min. The cell pellets were stored at −80 °C until use, and they were resuspended in a lysis buffer (50 mM sodium phosphate, 0.3 M NaCl, 10 mM imidazole, pH 7.4) and incubated with lysozyme at 100 μg/mL on ice for 10 min. Resuspended cell pellets were sonicated on ice for 15 min (10 s pulse-on and 20 s pulse-off). The cell lysate was centrifuged at 12,000 rpm for 40 min at 4 °C and then Ni-NTA resins were added to the supernatant followed by incubation for 30 min at 4 °C. The supernatant incubated with Ni-NTA resins was loaded on a polypropylene column and washed with washing buffer (50 mM sodium phosphate, 0.3 M NaCl, 20 mM imidazole, pH 7.4). After washing, UOX was eluted by elution buffer (50 mM sodium phosphate, 0.3 M NaCl, 250 mM imidazole, pH 7.4). The eluted UOX solution was buffer-exchanged with PBS buffer (pH 7.4) using a PD-10 column. UOX concentration was determined by absorbance measurement at 280 nm using a Synergy™ multimode microplate reader (BioTek, Winooski, VT, USA) according to the Beer-Lambert's law. The extinction coefficient of UOX was 53,520 M^{-1} cm^{-1}.

2.3. Determination of UA degradation rate by UOX

In order to optimize the ratio of UOX and AuNP, various concentrations of AuNPs (1, 2.5, 5, 10, 15, 20, and 25 μg/mL) were mixed with 500 nM of UOX. To determine the degradation rate of UA, 200 μM UA was mixed with UOX in PBS buffer (pH 7.4) and the absorbance at 293 nm was monitored using a Synergy™ multimode microplate reader. The extinction coefficient of UA at 293 nm was 12,300 M^{-1} cm^{-1}.

2.4. Preparation of UOX-AuNP@NCs

Pluronic based NCs were synthesized by photo-crosslinking the micelle state of diacrylated pluronic F127 (DA-F127), as previously reported [37,39]. Briefly, DA-PF127 was obtained by reacting pluronic with acyloyl chloride, and 10 wt% DA-F127 solution was prepared in deionized water (DIW). Then, 0.154 mL of the DA-F127 solution was added into 1.846 mL of DIW including 0.057 wt% irgacure 2959 to induce micelle formation of DA-F127. Using an ultraviolet (UV) lamp (VL-4.LC, 8 W, Vilber Lourmat, France), the mixed solution was irradiated for 15 min at 1.3 mW/cm^2 to perform the photo-crosslinking process for NC synthesis. The prepared NCs were purified by dialysis for 1 day using the spectra/Por dialysis membrane of MWCO 50 kDa and frequent change of the whole release buffer and lyophilized. UOX and AuNPs were co-encapsulated into the NCs (UOX-AuNP@NCs) using the temperature-dependent size change of the NCs [37,42]. Briefly, 1 mg of the NCs was dissolved in 1 mL of 5 μM UOX solution with 50 μg of AuNP. The mixture was incubated overnight at 4 °C to induce the size expansion of the NCs. Then, the temperature of the mixed solution was increased to 37 °C and maintained for 10 min to reduce the size of the NCs for encapsulation. The final solution was centrifuged using a nanosep® centrifugal device to remove the unloaded UOX and AuNPs (11,000 rpm, 37 °C, 10 min). After that, the amount of UOX in the UOX-AuNP@NCs was measured by bicinchoninic acid protein assay (Micro BCA protein assay kit, Thermo Fisher Scientific, Waltham, MA, USA). The loaded amount of AuNPs in the UOX-AuNP@NCs was calculated by absorbance of AuNPs at 525 nm using a spectrometer (Molecular Devices, Spectra-MaxM2e, Trenton, NJ, USA).

2.5. Size and surface charge of UOX-AuNP@NCs

The sizes and surface charges of NCs and UOX-AuNP@NCs were analyzed at 37 °C using an electrophoretic light scattering system (ELS-8000, Otsuka Electronics Osaka, Japan). Then, the stability of UOX-AuNP@NCs was determined by measuring the size change of UOX-AuNP@NCs at 1 mg/mL in a cell culture medium (RPMI 1640, Gibco, NY, USA) with 10% fetal bovine serum (FBS) at 37 °C and a 100 rpm environment [38]. The size of UOX-AuNP@NCs was observed at predetermined time points for 7 days.

2.6. Determination of in vitro UA degradation rate in NCs

In order to compare the UA degradation efficiencies, four enzyme systems were prepared as follows: (1) UOX, (2) UOX in NCs (UOX-NC), (3) UOX with AuNPs (UOX-AuNP), and (4) UOX-AuNP in NCs (UOX-AuNP@NC). Enzyme samples were incubated at 37 °C for 15 min and enzymatic assays of UOX at 10 nM were performed. 200 μL of assay buffer (50 mM sodium borate buffer, pH 8.0, 100 μM UA) was used and the UA degradation rates were calculated by measuring absorbance change at 293 nm.

2.7. Determination of H_2O_2 levels in vitro

Concentrations of H_2O_2 generated by UOX systems (UOX, UOX-AuNP, or UOX-AuNP@NC) upon the addition of UA into the samples were estimated using degradation of *N*,*N*-dimethyl-4-nitroaniline (RNO), as previously reported [43,45]. 0.25 M of RNO and 0.03 M of

histidine were prepared in DIW and mixed together. Then, UOX, UOX-NC, UOX-AuNP, or UOX-AuNP@NC solution was added into the RNO solution. The concentrations of UOX and UA were fixed at 200 nM and 1 mM, respectively. Then, H_2O_2 generation from each sample was measured by incubating the sample at room temperature for 10 min and observing *N*,*N*-dimethyl-4-nitroaniline (RNO) concentration by measuring absorbance at 440 nm.

2.8. In vitro cytotoxicity of UOX-AuNP@NC

Cytotoxicity of UOX-AuNP@NCs without UA was investigated using squamous cell carcinoma-7 (SCC7) cells obtained from American Type Culture Collection (Rockville, MD, USA) [46]. First, SCC7 cells were seeded at 5×10^3 cells/well in a 96-well tissue culture plate with a cell culture medium (RPMI 1640, Gibco, NY, USA) containing 10% FBS and 1% penicillin-streptomycin. The plated cells were incubated for 24 h at 37 °C with 5% CO_2 atmosphere condition. Then, the cells were washed using PBS buffer (pH 7.4) and treated with the prepared UOX-AuNP@NC samples at different concentrations (from 0 to 1 mg/mL on the basis of NC concentration). The sample treated cells were incubated overnight at 37 °C. Then, the cells were washed with PBS buffer and the cytotoxicity of the UOX-AuNP@NCs without UA was calculated using a Cell Counting Kit-8 (CCK-8, Dojindo Molecular Technologies, Inc., Kumamoto, Japan).

2.9. In vitro cytotoxicity determination of H_2O_2 generated by the UOX systems

To investigate the cytotoxicity of H_2O_2 generated by the UOX systems, the cytotoxicity of UOX-AuNP@NC in the presence of UA was compared to that of UOX and UOX-AuNP [32]. SCC7 cells were seeded at 5×10^3 cells/well in a 96-well tissue culture plate and cultured overnight at 37 °C in 5% CO_2 environment. The prepared cells were washed with PBS and treated with 100 μL of a sample such as UOX, UOX-NC, UOX-AuNP and UOX-AuNP @ NC. Each sample was processed to a final concentration of 200 nM UOX and 1 mM UA. Among them, UOX-NC was a negative control. The sample treated cells were incubated for 3 h at 37 °C and washed with PBS. The cytotoxicity of sample groups in the presence of UA was determined using a Cell Counting Kit-8.

2.10. Determination of in vivo uric acid level

For *in vivo* experiments, 8-week old, female C57BL/6 mice (Orient Bio Inc., Seongnam, South Korea) were used according to the guidelines of the Animal Care and Use Committee of the Gwangju Institute of Science and Technology (GIST) (Approval Number: GIST-2017-086).

To induce hyperuricemia state in the mice, they were treated with hypoxanthine and potassium oxonate, as previously reported [32]. Before the induction of hyperuricemia, all the mice were fasted overnight. Hypoxanthine was dissolved in 3% soluble starch solution and injected intragastrically into the mice at a dose of 475 μg/g. Then, potassium oxonate was dissolved in a co-solvent composed of a mixture of lanolin and liquid paraffin (3:2, v/v) and injected subcutaneously into the hypoxanthine treated mice at a dose of 95 μg/g. Five groups of mice were prepared: (1) normal mice compromising a negative control, (2) hyperuricemia mice compromising with no treatment, and hyperuricemia mice treated with (3) UOX, (4) UOX-AuNP, and (5) UOX-AuNP@NC (5). After that, 100 μL of sample solution (UOX concentration was fixed at 1 μM) either PBS, UOX, UOX-AuNP, or UOX-AuNP@NC was injected into the tail vein of the hyperuricemic mice. At predetermined time points (pre-induction and, 1, 3, 6, 12, and 18 h post-injection), blood was collected from the sample treated mice *via* retro-orbital bleeding [32]. At 18 h post-injection of samples, blood was collected by cardiac puncture [47]. The collected blood was centrifuged at 4 °C and 3000 rpm for 5 min to obtain serum. The UA concentration in the serum was analyzed after sample injection to compare the effect of UA degradation by the sample. For measuring the serum level of uric acid, samples were analyzed by the previously reported method [48] with little modification. Serum samples were subjected to an acid treatment using 0.3 M acetate buffer (pH 3.6) and then stored at 4 °C until analysis in order to prevent the degradation of uric acid by residual UOX (Fig. S5). Reagent mixtures for determination of serum UA were made in 0.3 M acetate buffer (pH 3.6) at a concentration of 0.83 mM 2,4,6-tripyridyl-s-triazine (TPTZ) and 1.66 mM $FeCl_3{\cdot}H_2O$. Absorbance at 593 nm was measured to determine the UA concentration. Also, in the presence or absence of NCs, the UA degradation rates of serum samples at 18 h post-injection were measured to estimate the residual activity of UOX.

3. Results and discussion

3.1. Preparation of purified UOX and AuNPs

Purified UOX was obtained as previously reported [24,44]. Briefly, the plasmid-encoding UOX gene (pQE80-UOX) was transformed into TOP10 *Escherichia coli* cells. The transformant TOP10_pQE80-UOX cells were cultured for expression of UOX. Cells expressing UOX were harvested and subjected to immobilized metal ion affinity chromatography using a hexahistidine affinity tag attached to UOX. The purity of UOX was > 95%, analyzed by SDS-PAGE analysis (Fig. S1(a)). The catalytic activity of purified UOX was confirmed using uric acid degradation assay (Fig. S1(b)).

Prior to NC encapsulation, the catalase-mimic catalytic activities of AuNPs were confirmed using H_2O_2 degradation assay (Fig. S1(c)), as previously reported [24].

3.2. Physiochemical properties and optimal ratio of UOX and AuNPs encapsulated in NCs

Pluronic-based NCs were used to deliver UOX and AuNPs simultaneously. UOX and AuNPs were co-encapsulated in NCs through temperature-dependent size changes. In order to achieve efficient UA degradation by UOX in the presence of AuNPs, the optimal ratio of UOX to AuNPs was investigated. Various concentrations of AuNPs (1, 2.5, 5, 10, 15, 20, and 25 μg/mL) were mixed with 500 nM UOX, and then encapsulated in NCs. In all cases, the loading efficiencies were over 90%, similar to protein loading in NCs in previous studies [37,42].

The enzymatic activity assay of samples showed that 5 μg/mL was the optimal concentration of AuNPs for efficient UA degradation (Fig. 2(a)). In the presence of 5 μg/mL AuNPs, the amount of UA degraded by UOX was 2.5 times higher compared than that by UOX alone. The simple and efficient loading of multiple components into pluronic-based NCs enabled us to modulate the composition of active components in the carrier and easily determine the optimal ratio between UOX and AuNPs. The proportion of UOX to AuNP was fixed at the optimal ratio in all subsequent experiments. In these conditions, the loading efficiency of UOX and AuNPs into the NCs was over 90% (92 ± 8% AuNPs and 93 ± 1% UOX, respectively).

Size and surface charge of the prepared NCs were characterized using an electrophoretic light scattering system at 37 °C to predict the size of NCs in the body. Without loading UOX and AuNPs, the size and surface charge of NCs were 67 ± 15 nm and − 4.2 ± 0.8 mV, respectively (Fig. 2b and c). After encapsulating UOX and AuNPs (UOX-AuNP@NC), the size and surface charge of UOX-AuNP@NCs were 65 ± 19 nm and − 5.1 ± 1.7 mV, respectively (Fig. 2b and c), indicating that there was no significant change in size and surface charge of NC upon loading of UOX and AuNPs. Efficient loading of AuNPs into NCs, instead of adsorption to the surface of NCs, was already confirmed in our previous report [37]. Furthermore, considering the predicted net charge of UOX as +1.4 at pH 7.4 (by Protein Calculator v3.3 developed by Dr. Chris Putnam at Scripps Research Institute), no increase but

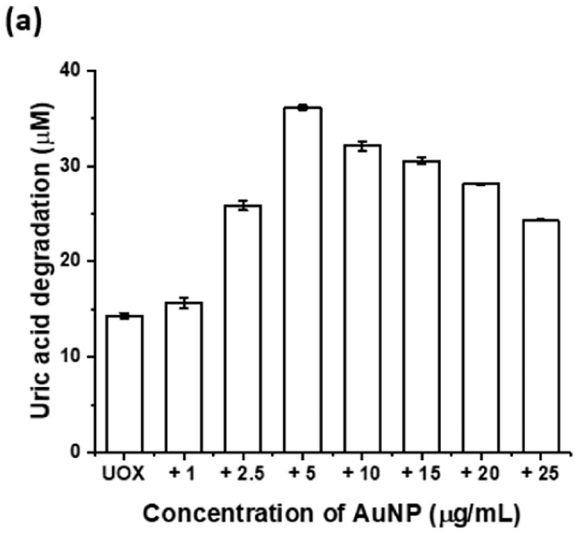

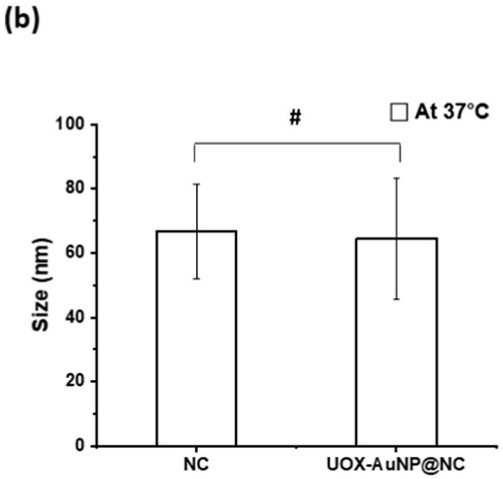

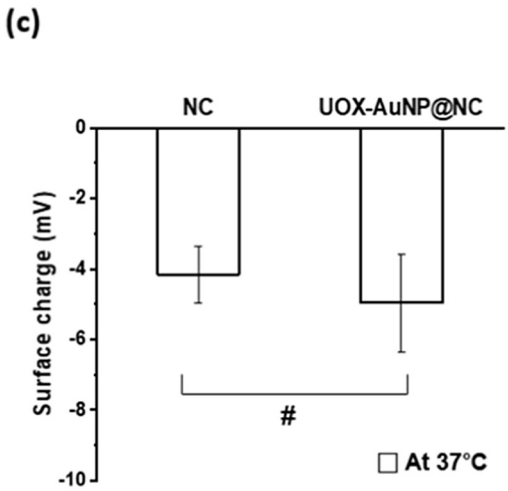

	PDI value
NC	0.26 ± 0.01
UOX-AuNP@NC	0.30 ± 0.01

Fig. 2. (a) UA degradation rate by UOX in the presence of varying concentrations of AuNPs encapsulated in NCs. (b) Size change of the NCs after loading UOX and AuNPs (UOX-AuNP@NC). (c) Surface charge of NCs and UOX-AuNP@NC. (#, $p > .05$ by *t*-test).

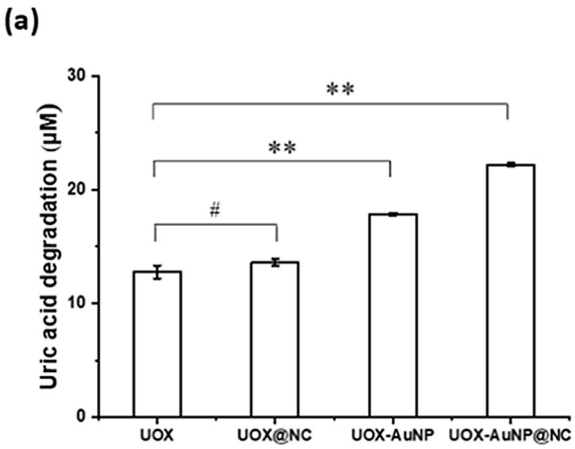

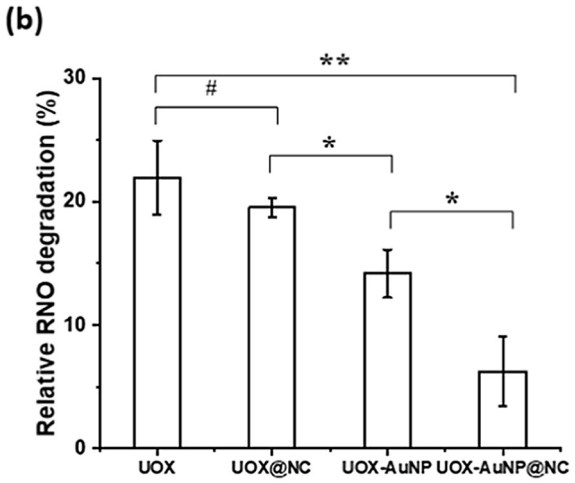

Fig. 3. Comparison of cascade reaction of UOX and AuNPs in different systems. (a) UA degradation assay. (b) Relative H_2O_2 production assay. ($^{\#}p > .05$, $^{*}p < .05$, $^{**}p < .01$ by *t*-test and ANOVA).

similar surface charge of NCs after loading both UOX and AuNPs supports that UOX was loaded inside the NCs as well as AuNPs, instead of adsorption to NC surfaces. In addition, UOX-AuNP@NC showed good size stability in a serum containing medium (10% serum, 37 °C, 100 rpm) up to 7 days (Fig. S2), implying colloidal stability *in vivo*. Considering that pluronic-based NCs can preserve protein activity and capture gold nanomaterials without perturbation of properties such as absorbance shift [37,40,42], we speculated that the physicochemical properties of UOX and AuNPs are not substantially affected by the encapsulation of UOX and AuNPs in the NCs. In Fig. 3(a), catalytic activity of UOX in NCs was not substantially reduced compared with that of free UOX. Similarly, the AuNPs in NCs exhibited catalytic activity comparable to that of free AuNPs (Fig. S3). Therefore, NCs are expected to simultaneously deliver UOX and AuNPs without compromising the critical properties under *in vivo* environment.

3.3. Enhanced catalytic activities of UOX encapsulated with AuNPs in NCs

We next analyzed the change in catalytic efficiency of UOX upon co-encapsulation with AuNPs in NCs. We hypothesized that the efficiency of catalytic activity will be enhanced by two factors. One is that the

addition of AuNPs will degrade a side-product H_2O_2, accelerating UA degradation reaction. The other is the proximity effect of multiple catalysts in cascade reactions [49]. Co-encapsulation of UOX and AuNPs in NCs will greatly reduce distances between UOX and AuNPs, accelerating H_2O_2 degradation *in situ*. In order to prove these hypotheses, we prepared four groups of enzyme systems including UOX alone (UOX), UOX encapsulated in NC (UOX@NC), free mixture of UOX and AuNPs (UOX-AuNP), and UOX and AuNPs encapsulated in NCs (UOX-AuNP@NC). The degraded amounts of UA and H_2O_2 were measured as previously reported [43]. As shown in Fig. 3(a), UA degradation rate of UOX and that of UOX@NC were similar. In the presence of AuNPs, UA degradation by UOX became 40% higher than that by UOX alone. In addition, UOX-AuNP@NC degraded 70% more UA than UOX alone.

Next, we investigated whether different enzyme systems led to different H_2O_2 levels during UA degradation *in vitro*. H_2O_2 levels were estimated by measuring RNO degradation (Fig. 3(b)). In the case of UOX alone, almost 20% of RNO was degraded *via* H_2O_2 produced from UA degradation by UOX [24,32]. Under the same reaction conditions, RNO degradation by UOX@NC was not significantly different from that by UOX alone. However, in the presence of AuNPs (UOX-AuNP), approximately 14% of RNO was degraded, indicating the lower H_2O_2 level. This result was consistent with our hypothesis of *in situ* degradation of H_2O_2 by AuNPs [24]. Interestingly, when both UOX and AuNP were loaded into NCs (UOX-AuNP@NC), only about 5% of RNO was degraded, implying more efficient removal of H_2O_2 than UOX-AuNP. These RNO degradation assay results (Fig. 3(b)) were well consistent with UA degradation assay results (Fig. 3(a)).

Similar UA degradation and H_2O_2 production by UOX alone and UOX@NC indicate that NCs themselves did not substantially affect the enzymatic activity of UOX. More importantly, these results imply that NCs do not hinder the transport of UA as well as H_2O_2 across NCs or inside NCs. Thus, NCs not only provided the efficient loading of enzyme and nanoparticles, but also allowed the transport of small molecules including substrate and product for enzymatic reaction across or inside the carrier, which is a key requirement for proper action of delivered enzymes against target molecules present inside the body. A significant increase in the UA degradation and a significant decrease in H_2O_2 level of UOX-AuNP@NC compared to UOX-AuNP imply that NCs did not hinder the cascade reactions between them. Also, these results demonstrate our hypothesis of the proximity effect made by co-localizing UOX and AuNPs in NCs on H_2O_2 removal and UA degradation. We speculated that the distances between UOX and AuNPs were closer in NCs than those between free mixture of UOX and AuNPs. Considering that blood volume is much greater than sample injection volume, samples are expected to be substantially diluted *in vivo* upon administration. Therefore, the more pronounced effect of co-encapsulation of UOX and AuNPs in NCs on H_2O_2 removal and UA degradation would be expected *in vivo*. Thus, we confirmed the favorable features of our delivery platform for the enhanced efficacy but reduced side product of a therapeutic protein with the ultimate goal of clinical applications.

3.4. In vitro cytotoxicity of UOX-AuNP@NC with or without UA

Before *in vivo* experiment using UOX-AuNP@NC, cytotoxicity of UOX-AuNP@NC without UA was measured to verify the biosafety of the nanosystem using SCC7 cancer cells (Fig. 4a). Cytotoxicity was indicated by reduction in the cellular activity. The assay results showed that UOX-AuNP@NC without UA exhibited no cytotoxicity up to 1 mg/mL based on the NC concentration. Considering that NCs themselves have no *in vitro* toxicity [39], AuNP does not have severe toxicity issue, and UOX can produce toxic substance such as H_2O_2 only in the presence of UA [24], UOX-AuNP@NC, containing both UOX and AuNP inside the pluronic based NC, is expected to be safe without significant toxicity in the absence of UA.

In order to evaluate H_2O_2-related cytotoxicity, cytotoxicity of UOX-AuNP@NC system was compared to those of other samples in the presence of UA (Fig. 4b). SCC7 cancer cell line was used because cancer cells are more susceptible to reactive oxygen species such as H_2O_2 accumulation than normal cells [50]. As expected, UA alone samples (UA (+)) did not show any significant cytotoxicity, similar to negative control samples without UA (UA (−)). In contrast, in the presence of UA, UOX samples showed significant (about 70%) cell death due to the produced H_2O_2. Encapsulation of UOX in NCs (UOX@NC) did not significantly reduce the cytotoxicity, similar to the results of H_2O_2 production (Fig. 3b). On the other hand, UOX and AuNPs dissolved solution (UOX-AuNP) samples showed the significantly reduced cytotoxicity (about 40%) due to H_2O_2 removal by AuNPs in the closed experimental setup. More importantly, UOX-AuNP@NC showed further reduced cytotoxicity compared to UOX-AuNP. The cellular activity of UOX-AuNP@NC samples was very high, and was even comparable to that of the control UA (−). All of these results were well consistent with the results of UA degradation assay (Fig. 3a) and H_2O_2 production assay (Fig. 3b). Also, these results suggest that H_2O_2 generated by UOX during UA degradation can cause toxicity, a potential side-effect in *in vivo* clinical applications, however efficient removal of H_2O_2 by UOX-AuNP@NC can mitigate the toxicity issue of H_2O_2 produced by UOX.

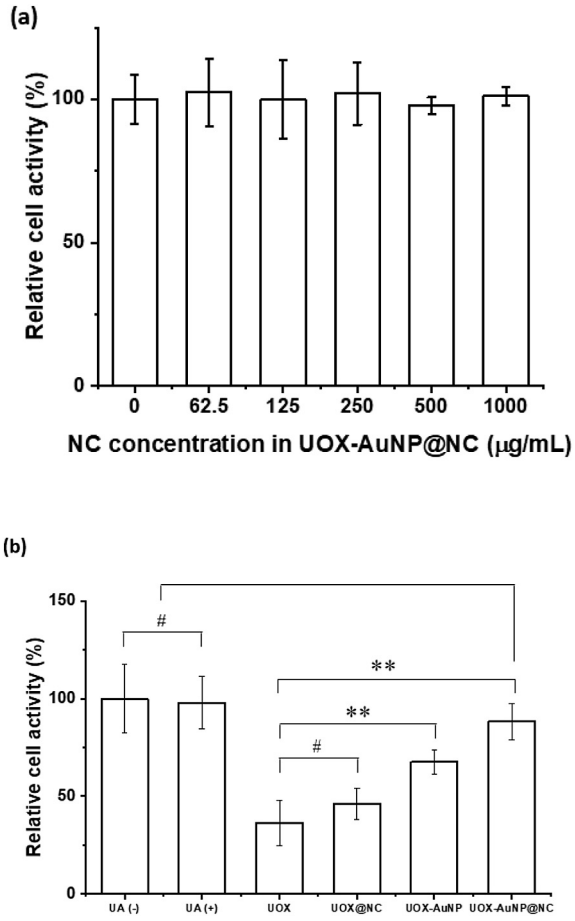

Fig. 4. (a) Cytotoxicity of UOX and AuNP loaded NC without UA. (b) Cytotoxicity of various systems induced by H_2O_2 with UA. (#$p > .05$, *$p < .05$, **$p < .01$ by *t*-test and ANOVA).

3.5. Evaluation of in vivo activities of UOX and AuNP loaded NC

To characterize the therapeutic effect of UOX-AuNP@NC *in vivo*, a hyperuricemia mouse model was used, as shown in Fig. 5a. Mice were divided into 5 groups: normal control (Control), hyperuricemia (Hyperuricemia), UOX treated (UOX), UOX-AuNP treated (UOX-AuNP),

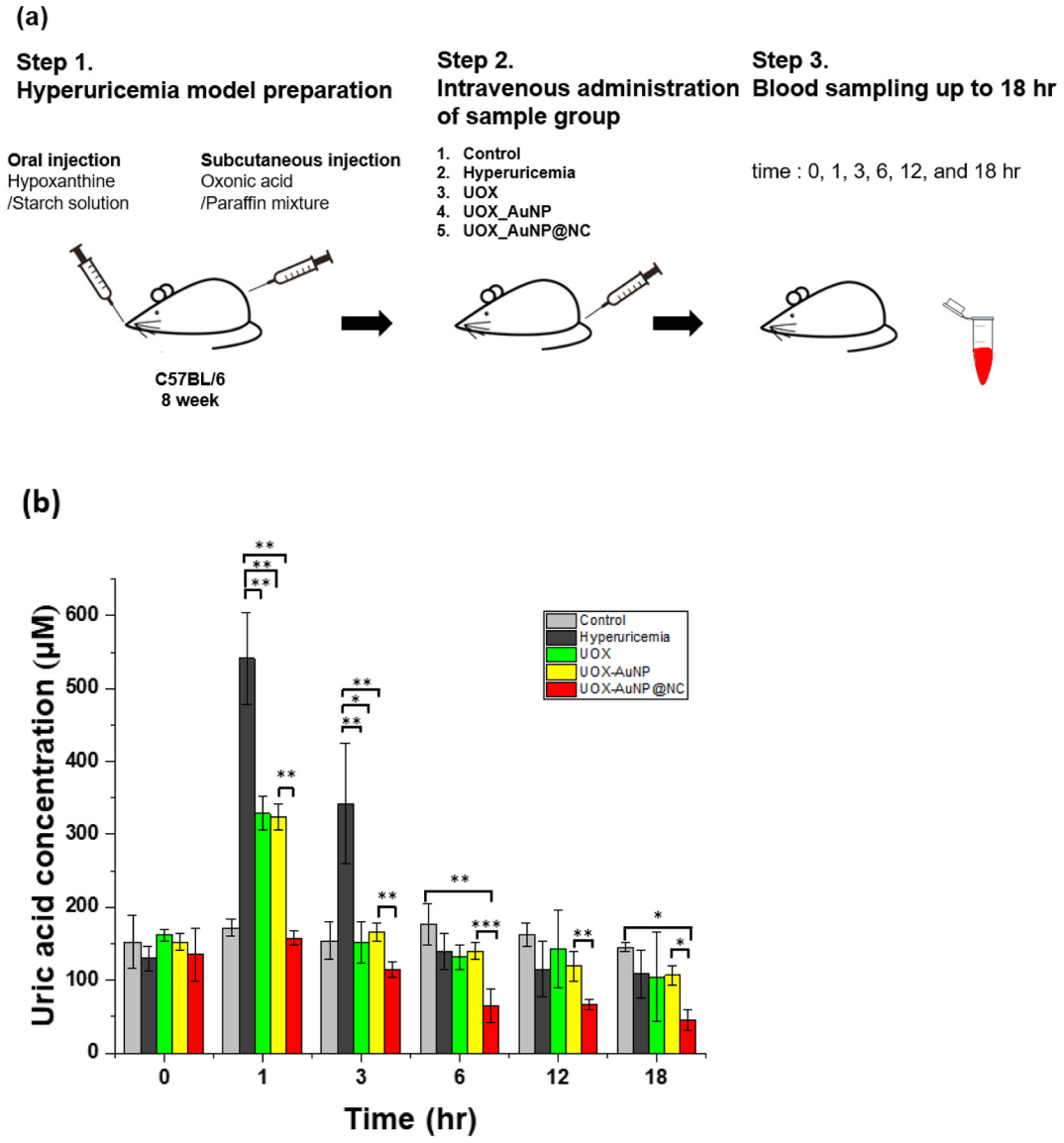

Fig. 5. (a) Experimental scheme of therapeutic effect in different enzyme system. (b) Therapeutic effect of 5 different treatment groups. (#$p > .05$, *$p < .05$, **$p < .01$, ***$p < .001$ by t-test).

and UOX-AuNP@NC treated (UOX-AuNP@NC) groups. C57BL/6 hyperuricemia mice were injected with UOX, UOX-AuNP, or UOX-AuNP@NC by intravenous administration with the same amount of enzyme. Blood samples obtained at predetermined time points were analyzed and the concentrations of UA were determined (Fig. 5b) using a calibration curve (Fig. S4b).

First, among experimental groups, hyperuricemia group showed a much higher (over 3 folds) UA concentration in serum at 1 h compared to the pre-induction (0 h) or the normal control (no hyperuricemia induction) group (Fig. 5b). At 3 h after induction, still over 2 fold increase in UA concentration was observed for hyperuricemia group compared to pre-induction (0 h) or the normal control group. From 6 h post-induction, hyperuricemia group showed similar UA concentrations in serum compared to that of the control group or the pre-induction state. Thus, our method of hyperuricemia induction induced an increase in the UA concentration initially, then lasted at least up to 3 h. This temporal effect on hyperuricemia was also reported in previous reports using the similar induction method [32]. In contrast, UOX-treated groups (UOX, UOX-AuNP, and UOX-AuNP@NC) all showed significantly lower concentrations of UA in serum than that of the hyperuricemia group at both 1 h and 3 h, confirming the UA degradation by UOX *in vivo*. Among UOX-treated groups, UOX and UOX-AuNP showed very similar UA concentrations (similar UA degradation) whereas UOX-AuNP@NC showed significantly lower concentration of UA than UOX and UOX-AuNP, revealing a superior UA degradation by UOX-AuNP@NC compared to UOX and UOX-AuNP (Fig. 5b). The similar effect of UOX and UOX-AuNP suggests that simple mixing and co-injection of UOX and AuNP was not sufficient to achieve the cascade reaction of UOX and AuNP *in vivo*. So, as expected, dilution after injection seemed to prevent the co-localization of UOX and AuNP *in vivo*. In contrast, much more effective decomposition of UA by UOX-AuNP@NC compared to UOX and UOX-AuNP proved that co-delivery of UOX and AuNP by of NC encapsulation could make a sufficient environment for the cascade reaction to occur in blood.

In addition, at 6 h or later, UOX and UOX-AuNP showed similar UA concentrations compared to the normal or hyperuricemia group in contrast to the maintenance of lower concentration of UA for UOX-AuNP@NC group, indicating that the UA degradation by UOX was effective until 18 h for UOX-AuNP@NC group only (Fig. S6). In order to understand the prolonged activity of UOX for UOX-AuNP@NC group, the serum half-life of NCs was determined using Cy5.5 labeled NCs in mice (Fig. S7). Since the decay rate of serum concentration showed a

sharp transition, a two-phase model was used to analyze the data. The serum half-life of NC for the alpha-phase was about 0.64 h, and the serum half-life of NCs for beta-phase (~ 13 h) was significantly longer than serum half-life of free UOX (~1.4 h) [44]. Another experiment was performed to evaluate the body distribution of injected NCs, and the result showed that NCs were distributed predominantly in the liver at 6 h post intravenous administration (Fig. S8). Thus, the extended half-life of NC for beta-phase could be explained by the slow elimination of NCs from the body. Therefore, it can be postulated that the extended uric acid degradation activity of UOX co-encapsulated with AuNPs in NCs resulted from the extended half-life of NCs encapsulating UOX. Furthermore, UOX and AuNPs co-encapsulated in NCs exhibited a greater uric acid degradation activity than free mix of UOX and AuNPs at early time points *in vivo* (Fig. 5). These results suggest that the relatively longer half-life of NCs compared to free UOX and the enhanced UOX activity by AuNPs co-encapsulated in NCs were attributed to the extended uric acid degradation activity.

As previously reported [24], clearance of toxic intermediate H_2O_2 can facilitate UA degradation. Also, the effective removal of H_2O_2 by UOX-AuNP@NC can lower the toxicity issue associated with H_2O_2. To analyze the toxicity of the present system, histopathological changes in the major visceral organs at 48 post intravenous administration of each sample (saline, UOX, UOX-AuNP, and UOX-AuNP@NC) into healthy mice were observed (Fig. S9). Hematoxylin/eosin (H&E) staining of tissue sections showed mild congestion in the kidney for both UOX and UOX-AuNP group whereas UOX-AuNP@NC group showed no difference compared to the control sample (saline injection). Periodic acid–Schiff (PAS) staining of the kidney samples was used to further analyze the injured state in the kidney sections, and it confirmed tissue damage for both UOX and UOX-AuNP whereas no discernable pathological lesion was observed for UOX-AuNP@NC as well as the control group. These results imply that H_2O_2 produced by UOX may cause some toxicity in the kidney *in vivo* and the H_2O_2-associated toxicity was not effectively eliminated by free mixing of AuNPs with UOX. In contrast, AuNPs co-encapsulated with UOX in NCs could substantially reduce the associated toxicity. The results also support that NCs encapsulating UOX and AuNPs did not cause noticeable toxicity issue. Thus, combing with significantly better UA degradation effect by co-delivering UOX and AuNP using NC (UOX-AuNP@NC) *in vivo*, our delivery platform has an obvious clinical potential for hyperuricemia treatment through synergistic effect of UOX and AuNPs.

4. Conclusion

From characterization of physical and catalytic properties of pluronic based nanocarriers (NCs), it was shown that biocompatible NCs could encapsulate both therapeutic protein (UOX) and enzyme-mimic nanoparticles (AuNPs) in a high loading efficiency (> 90%) by simple temperature-dependent size changes. Loading of UOX and AuNPs into the NCs did not affect the physical properties (size and surface charge) of NCs. NCs themselves did not alter the enzymatic activity of UOX, and did not hinder the transport of substrate and product of the reaction across the NCs, either. In addition, easy and efficient loading of enzyme and enzyme-mimic nanoparticles into the NCs led to modulation of a mixing ratio between UOX and AuNPs for optimal efficacy. Co-localizing UOX and AuNPs in the NCs led to the enhanced UA degradation and H_2O_2 removal *in vitro*. In addition, such an enhanced H_2O_2 removal by co-encapsulation of UOX with AuNPs in NCs greatly reduced the H_2O_2-associated cytotoxicity in cultured cells compared with UOX alone or a free mixture of UOX and AuNPs. Finally, we demonstrated that co-delivery of UOX and AuNPs using NCs could significantly improve the *in vivo* UA degradation compared to simple coinjection of UOX and AuNPs without NCs, suggesting a promise for therapeutic applications. Co-delivery of multicompoments using NCs will be applicable to achieve efficient cascade reactions in various systems.

Acknowledgements

The authors acknowledge the financial support from the National Research Foundation of Korea (NRF) funded by the Ministry of Science, ICT & Future Planning (Grant No. 2018R1A4A1024963).

Appendix A. Supplementary data

Supplementary data to this article can be found online at https://doi.org/10.1016/j.jconrel.2019.07.038.

References

[1] D.J.A. Crommelin, G. Storm, R. Verrijk, L. De Leede, W. Jiskoot, W.E. Hennink, Shifting paradigms: biopharmaceuticals versus low molecular weight drugs, Int. J. Pharm. 266 (2003) 3–16.
[2] L.S. Garcia, L. Martín, R. Mangues, N.F. Miralles, E. Vázquez, A. Villaverde, Recombinant pharmaceuticals from microbial cells: a 2015 update, Microb. Cell Factories 15 (2016) 33.
[3] H.A.D. Lagassé, A. Alexaki, V.L. Simhadri, N.H. Katagiri, W. Jankowski, Z.E. Sauna, C. Kimchi-sarfaty, Recent advances in (therapeutic protein) drug development, F1000Res. 6 (2017) 113.
[4] Z. Vajo, J. Fawcett, W.C. Duckworth, Recombinant DNA technology in the treatment of diabetes: insulin analogs, Endocorine Rev. 22 (2001) 706–717.
[5] A.H. Boekhout, J.H. Beijnen, J.H.M. Schellens, Trastuzumab, Oncologist 16 (2011) 800–810.
[6] J.S. Sundy, N.J. Ganson, S.J. Kelly, E.L. Scarlett, C.D. Rehrig, W. Huang, M.S. Hershfield, Pharmacokinetics and pharmacodynamics of intravenous PEGylated recombinant mammalian urate oxidase in patients with refractory gout, Arthritis Rheum. 56 (2007) 1021–1028.
[7] S. Mitragotri, P.A. Burke, R. Langer, Formulation and delivery strategies, Nat. Publ. Gr. 13 (2014) 655–672.
[8] L.M. Ortega, G. Contreras, The clinical impact of the physiological effects of erythropoietin and erythropoietin-stimulating agents on the incidence of malignancy, thrombosis and hypertension: beyond anaemia, Nefrlogia. 29 (2009) 288–294.
[9] M. Krishna, S.G. Nadler, Immunogenicity to biotherapeutics –the role of anti-drug immune complexes, Front. Immunol. 7 (2016) 21.
[10] B. Baldo, B.A. Baldo, Adverse events to monoclonal antibodies used for cancer therapy: focus on hypersensitivity responses, Oncoimmunology. 2 (2013) e26333.
[11] J.C. Egrie, J.K. Browne, Development and characterization of novel erythropoiesis stimulating protein (NESP), Br. J. Cancer 84 (2001) 3–10.
[12] M. Parsons, N. Spratt, A. Bivard, B. Sc, B. Campbell, K. Chung, F. Miteff, B.O. Brien, C. Bladin, P. Mcelduff, D. Ph, C. Allen, G. Bateman, G. Donnan, S. Davis, C. Levi, A randomized trial of tenecteplase versus alteplase for acute ischemic stroke, N. Engl. J. Med. 366 (2012) 1099–1107.
[13] E.M.P. Day, E. Lin, H.D. Maynard, Therapeutic protein − polymer conjugates: advancing beyond PEGylation, J. Am. Chem. Soc. 136 (2014) 14323–14332.
[14] R. Duncan, Polymer therapeutics as nanomedicines: new perspectives, Curr. Opin. Biotechnol. 22 (2011) 492–501.
[15] J.T. Hardwicke, J. Hart, A. Bell, R. Duncan, D.W. Thomas, R. Moseley, The effect of dextrin – rhEGF on the healing of full-thickness, excisional wounds in the (db/db) diabetic mouse, J. Control. Release 152 (2011) 411–417.
[16] S. Jain, D.H. Hreczuk-hirst, B. Mccormack, M. Mital, Polysialylated insulin: synthesis, characterization and biological activity in vivo, Biochim. Biophys. Acta 1622 (2003) 42–49.
[17] S.D. Chipman, Biological and clinical characterization of paclitaxel poliglumex (PPX, CT-2103), a macromolecular polymer – drug conjugate, Int. J. Nanomedicine 1 (2006) 375–383.
[18] S.P. Juraschek, L.C. Kovell, E.R. Miller, A.C. Gelber, Dose-response association of uncontrolled blood pressure and cardiovascular disease risk factors with hyperuricemia and gout, PLoS One 8 (2013) e56546.
[19] R.J. Johnson, T. Nakagawa, D. Jalal, L.G. Sánchez-Lozada, D.H. Kang, E. Ritz, Uric acid and chronic kidney disease: which is chasing which? Nephrol. Dial. Transplant. 28 (2013) 2221–2228.
[20] A.L. Gaffo, N.L. Edwards, K.G. Saag, Gout. Hyperuricemia and cardiovascular disease: how strong is the evidence for a causal link? Arthritis Res. Ther. 11 (2009) 1–7.
[21] C. Kuo, M.J. Grainge, W. Zhang, M. Doherty, Global epidemiology of gout: prevalence, incidence and risk factors, Nat. Publ. Gr. 11 (2015) 649–662.
[22] C. Pui, S. Jeha, D. Irwin, B. Camitta, Recombinant urate oxidase (rasburicase) in the prevention and treatment of malignancy-associated hyperuricemia in pediatric and adult patients: results of a compassionate-use trial, Leukemia. 15 (2001) 1505–1509.
[23] W. He, Y. Zhou, W.G. Wamer, X. Hu, X. Wu, Z. Zheng, M.D. Boudreau, J. Yin, Biomaterials intrinsic catalytic activity of Au nanoparticles with respect to hydrogen peroxide decomposition and superoxide scavenging, Biomaterials 34 (2013) 765–773.
[24] S. Jung, I. Kwon, Synergistic degradation of a hyperuricemia-causing metabolite using one-pot enzyme-nanozyme cascade reactions, Sci. Rep. 7 (2017) 44330.
[25] X. Wang, Y. Hu, H. Wei, Nanozymes in bionanotechnology: from sensing to therapeutics and beyond, Inorg. Chem. Front. 3 (2016) 41–60.
[26] Hui Wei, Erkang Wang, Nanomaterials with enzyme-like characteristics

(nanozymes): next-generation artificial enzymes, Chem. Soc. Rev. 42 (2013) 6060–6093.
[27] J. Wu, S. Li, H. Wei, Integrated nanozymes: facile preparation and biomedical applications, Chem. Commun. 54 (2018) 6520–6530.
[28] A. Banstola, J. Jeong, Current applications of gold nanoparticles for medical imaging and as treatment agents for managing pancreatic cancer, Macromol. Res. 26 (2018) 955–964.
[29] Y.D. Suh, J.H. Park, PEGylated gold nanoprobe bearing the diselenide bond for ROS-responsive fluorescence imaging, Macromol. Res. 26 (2018) 577–580.
[30] J.R. Seo, D.E. Kim, D.Y. Park, E. Kim, B.G. Chung, Facile synthesis of surfactant-free Au decorated hollow silica nanoparticles for photothermal applications, Macromol. Res. 26 (2018) 1129–1134.
[31] Y. Hu, H. Cheng, X. Zhao, J. Wu, F. Muhammad, S. Lin, J. He, L. Zhou, C. Zhang, Y. Deng, P. Wang, Z. Zhou, S. Nie, H. Wei, Surface-enhanced raman scattering active gold nanoparticles with enzyme-mimicking activities for measuring glucose and lactate in liver tissues, ACS Nano 11 (2017) 5558–5566.
[32] X. Liu, Z. Zhang, Y. Zhang, Y. Guan, Z. Liu, J. Ren, Artificial metalloenzyme-based enzyme replacement therapy for the treatment of hyperuricemia, Adv. Funct. Mater. 26 (2016) 7921–7928.
[33] C. Tamames-tabar, D. Cunha, E. Imbuluzqueta, F. Ragon, C. Serre, Cytotoxicity of nanoscaled metal–organic frameworks, J. Mater. Chem. B 2 (2014) 262–271.
[34] Q. He, Z. Zhang, Y. Gao, J. Shi, Y. Li, Intracellular localization and cytotoxicity of spherical mesoporous silica nano- and microparticles, Small 5 (2009) 2722–2729.
[35] I.I. Slowing, C. Wu, J.L. Vivero-escoto, V.S. Lin, Mesoporous silica nanoparticles for reducing hemolytic activity towards mammalian red blood cells, Small 5 (2009) 57–62.
[36] N. Judge, L. Wang, Y. Wang, Molecular engineering of metal-organic cycles/cages for drug delivery, Macromol. Res. 26 (2018) 1074–1084.
[37] W. Il Choi, G. Tae, Y.H. Kim, One pot, single phase synthesis of thermo-sensitive nano-carriers by photo-crosslinking of a diacrylated pluronic, J. Mater. Chem. 18 (2008) 2769–2774.
[38] M. Kim, A. Sahu, G.B. Kim, G.H. Nam, W. Um, S.J. Shin, Y.Y. Jeong, I.S. Kim, K. Kim, I.C. Kwon, G. Tae, Comparison of in vivo targeting ability between cRGD and collagen-targeting peptide conjugated nano-carriers for atherosclerosis, J. Control. Release 269 (2018) 337–346.
[39] J. Kim, W. Il, Y. Ha, G. Tae, S. Lee, K. Kim, I. Chan, In-vivo tumor targeting of pluronic-based nano-carriers, J. Control. Release 147 (2010) 109–117.
[40] W. Il Choi, J.-Y. Kim, C. Kang, C.C. Byeon, Y.H. Kim, G. Tae, Tumor regression in vivo by photothermal therapy based on gold-nanorod-loaded, functional nano-carriers, ACS Nano 5 (2011) 1995–2003.
[41] W. Il Choi, J.-Y. Kim, S.U. Heo, Y.Y. Jeong, Y.H. Kim, G. Tae, The effect of mechanical properties of iron oxide nanoparticle-loaded functional nano-carrier on tumor targeting and imaging, J. Control. Release 162 (2012) 267–275.
[42] I. Choi, Y.H. Kim, G. Tae, Controlled release of proteins from pluronic-based nano-carrier, Macromol. Res. 19 (2011) 639–642.
[43] J. Kim, W.I. Choi, M. Kim, G. Tae, Tumor-targeting nanogel that can function independently for both photodynamic and photothermal therapy and its synergy from the procedure of PDT followed by PTT, J. Control. Release 171 (2013) 113–121.
[44] S. In, Y.S. Hahn, I. Kwon, Site-specific albumination of a therapeutic protein with multi-subunit to prolong activity in vivo, J. Control. Release 207 (2015) 93–100.
[45] I.J. MacDonald, T.J. Dougherty, Basic principles of photodynamic therapy, J. Porphyrins Phthalocyanines 5 (2001) 105–129.
[46] M. Kim, J.H. Lee, S.E. Kim, S.S. Kang, G. Tae, Nanosized ultrasound enhanced-contrast agent for in vivo tumor imaging via intravenous injection, ACS Appl. Mater. Interfaces 8 (2016) 8409–8418.
[47] S. Parasuraman, R. Raveendran, R. Kesavan, Blood sample collection in small laboratory animals, J. Pharmacol. Pharmacother. 1 (2010) 87–93.
[48] I.F.F. Benzie, J.J. Strain, The ferric reducing ability of plasma (FRAP) as a measure of " antioxidant power": the FRAP assay, Anal. Biochem. 239 (1996) 70–76.
[49] A. Küchler, M. Yoshimoto, S. Luginbühl, F. Mavelli, P. Walde, Enzymatic reactions in confined environments, Nat. Nanotechnol. 11 (2016) 409–420.
[50] J. Liu, Z. Wang, Increased oxidative stress as a selective anticancer therapy, Oxidative Med. Cell. Longev. 2015 (2015) 294303.